Cascade DNA Structural Transitions Enable Stimuli-Responsive Hydrogels

*Michael Shao Min Ho,[1,2‡] Alycia Zi Ting Lim,[1,3‡] Yujie Ke,[4] Wei Wei Loh,[1] Xin Ting Zheng,[1] Le Yang,[1] Zhaogang Dong,[1,5] Fuke Wang,[1] Jason Y. C. Lim,[1] Yuwei Hu[1]**

1. Institute of Materials Research and Engineering (IMRE), Agency for Science, Technology and Research (A*STAR), 2 Fusionopolis Way, Innovis #08-03, 138634 Singapore, Republic of Singapore

2. Department of Chemistry, National University of Singapore, 3 Science Drive 3, Singapore 117543, Republic of Singapore

3. College of Design and Engineering, National University of Singapore, 21 Lower Kent Ridge Road, 119077 Singapore, Republic of Singapore

4. School of Interdisciplinary Studies, Lingnan University, Tuen Mun, Hong Kong SAR 999077, China.

5. Science, Mathematics, and Technology (SMT), Singapore University of Technology and Design (SUTD), 8 Somapah Road, Singapore 487372, Republic of Singapore.

KEYWORDS: cofactor, melamine, noncanonical, adenine, thymine.

ABSTRACT

Cascade interactions are fundamental to enzyme catalysis and cellular activities, enabling dynamic and adaptive responses to environmental stimuli. DNA-based cascade systems have been widely employed to mimic biological processes, such as immune responses and DNAzyme catalysis, achieved mainly through hybridization interaction. Herein, we present a cascade DNA system involving single-stranded sequences, noncanonical cofactor-bridged duplexes, and canonical duplexes to construct and dissociate hydrogel matrices. In this work, thymine-rich oligonucleotides (T-strands) exist as single-stranded random coils in a buffer at pH 7.2. Upon the introduction of a low-molecular-weight cofactor, melamine (MA), a supramolecular noncanonical configuration, termed T-MA-T duplex, is formed. Subsequent addition of adenine-rich oligonucleotides (A-strand) to the system leads to the replacement of MA cofactors and the formation of more energetically favourable canonical A-T duplex structures. These consecutive structural transitions are further utilized as dynamic bridging elements in stimuli-responsive DNA hydrogels, facilitating liquid-hydrogel-liquid phase transitions. Moreover, we demonstrate precisely controlled release profiles of doxorubicin from the DNA hydrogel. This approach, leveraging both noncanonical and canonical DNA configurations in triggered cascade structural transitions, opens avenues for developing molecular switches, electronic nanodevices, adaptive materials, and other advanced applications.

INTRODUCTION

Cascade interactions play a pivotal role in various research aspects. For example, substrate transportation/information processing among the organelles of cells, their resemblance by developing multi-compartmentalized polymersomes,[1] catalytic interactions via multiple enzymes,[2] total synthesis in organic chemistry,[3] and others have been developed. Among these designs,

DNA-mediated cascade interactions have garnered significant research attention in recent years, stemming from DNA's exceptional programmability, designability, specific recognition capabilities through base-pairing or aptamer-ligand complexes, and responsiveness to diverse external stimuli (e.g., light, pH, ions), etc. These attributes position DNA as an ideal candidate for constructing versatile platforms with cascade functionalities.

Recent advances in DNA-based cascade systems include innovative applications, such as hairpin DNA cascade reaction for mRNA imaging within live cells,[4,5] DNA cascade networks mimicking the adaptive immune response,[6] DNA-mediated multiple enzymes/DNAzyme catalysis,[7-10] DNA origami domino array,[11] DNA-based plasmonic nanodevices,[12] DNA-facilitated clustering of catalytic nanocompartments,[13] DNA circuits for gene silencing,[14] constitutional dynamic networks,[15-22] etc. Additionally, as polymeric supramolecules with specific recognition and secondary-structure formation capabilities, cascade DNA configurations have also been exploited in stimuli-responsive hydrogels demonstrating shape-swelling,[23,24] therapeutics delivery,[25-27] hydrogel-liquid transitions,[28] and more. These structural transitions are typically achieved through hybridization chain reactions involving DNA hairpins or stimuli-triggered switching of multiconfiguration systems. Beyond pure DNA derived noncanonical structures, the integration of low-molecular-weight cofactors, such as cyanuric acid (CA) or melamine (MA), has facilitated the assembly of DNA strands into sophisticated supramolecular frameworks,[29] such as triplexes. Such assemblies have been applied to the programming of polymeric fibers,[30-33] the formation of nanostructures,[34] the development of stiff hydrogels for gene silencing,[35] and the assembly or disassembly of macroscopic objects.[36] The incorporation of these cofactors significantly enhances the versatility of DNA toolkits, broadening their applications beyond those of pure DNA structures.

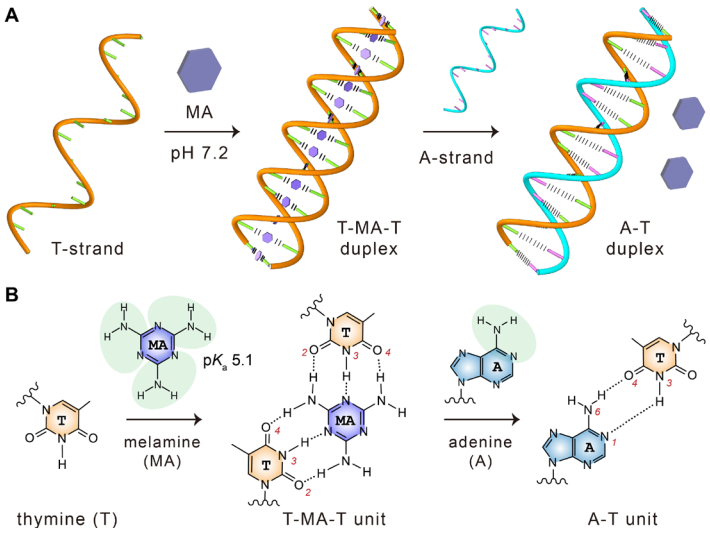

Figure 1. (A) Schematic representation of the MA-facilitated assembly of single T-strands into supramolecular noncanonical T-MA-T duplexes, followed by their transition into canonical A-T duplexes through Watson-Crick base-pairing. (B) Chemical structures of thymine (T), the MA cofactor with three adenine-like faces, a T-MA-T unit utilizing two faces of the MA cofactor, adenine (A) and an A-T unit exhibiting Watson-Crick base-pairing

In this study, we present a consecutive cascade structural transition by integrating both noncanonical and canonical DNA configurations derived from thymine-rich strands (T-strands). This system transitions through three distinct states: single-coil T-strands, melamine (MA)-induced noncanonical T-MA-T duplexes, and canonical A-T duplexes formed through hybridization with adenine-rich strands (A-strands). Specifically, T-strands exist as single strands under neutral conditions. Upon the introduction of MA cofactors, which possess adenine-like structural features, the T-strands assemble into noncanonical T-MA-T duplexes stabilized by hydrogen bonding. These duplexes subsequently transition into canonical A-T duplexes upon the addition of A-strands, which displace the MA cofactors due to the stronger Watson-Crick A-T base-pairing affinity (Figure 1A). Furthermore, the cascade structural switching of T-strand-

derived frameworks has been developed into a stimuli-responsive DNA copolymer, exhibiting consecutive phase transitions across liquid-hydrogel-liquid states. The dissociation profiles of the hydrogel, formed by noncanonical T-MA-T duplexes, and the controlled release of encapsulated payloads are precisely modulated by MA cofactors or A-strands. These features make it distinguished from our previous study,[36] in which T-MA-T duplexes functioned as crosslinkers in a multi-stimuli responsive DNA hydrogel and as nanobridges for the programmable assembly/disassembly of macroscopic hydrogel cubes. The integration of both noncanonical and canonical DNA frameworks within a single system, combined with stimuli-triggered cascade structural transitions, hold potential for innovative applications in smart functional materials, molecular switches, electronic devices, controlled cargo release, and more.

RESULTS AND DISCUSSION

MA cofactors possess three adenine-like faces (Figure 1B), which can theoretically induce the assembly of three T-strands via hydrogen bonding. However, the results from native polyacrylamide gel electrophoresis, dynamic light scattering, circular dichroism (CD), and Job plot revealed the formation of T-MA-T duplex, instead of a triplex, due to the steric hindrance and strong electric repulsion among T-strands.[34] In addition, X-ray crystallography analysis verified a right-handed, antiparallel duplex comprising consecutive T-MA-T units.[34] In this structure, the MA cofactor forms three hydrogen bonds with each thymine, involving the O2, N3 and O4 atoms, arranged in an approximately coplanar configuration.[34] The geometry and hydrogen-bond lengths are comparable to those observed in a noncanonical C^+·G-C triplex configuration,[37] where the MA cofactor substitutes for guanine (G) and T takes the place of protonated cytosine (C^+) and cytosine (C).

The formation of the T-MA-T duplex was investigated using UV-Vis spectroscopy. As illustrated in Figure 2A, a 21-mer T-strand (T21) exhibits a characteristic DNA spectrum, with a maximum absorbance at 266nm. In contrast, MA cofactors show absorption behaviour primarily at wavelengths below 260nm. Upon the addition of MA cofactors to T21, a significant hypochromic effect was observed, demonstrating base-stacking interactions within T21 and the formation of T-MA-T antiparallel duplex. Notably, the T-MA-T duplex was formed under various ionic strengths (e.g., 1×PBS with 10 mM $MgCl_2$, 0.5×PBS with 5 mM $MgCl_2$, 0.1×PBS with 1mM $MgCl_2$) and even in distilled water (Figure 2A). The hypochromic effect indicates the formation of T-MA-T duplex, with ΔAbs_{266nm} values of approximately 0.12 in all PBS buffers with ions, while a slightly lower ΔAbs_{266nm} value of 0.1 was observed in distilled water. This result highlights the strong affinity between the MA cofactor and T21 strands, even in the absence of ions. However, in the following studies, 1×PBS was used to mimic the physiological conditions, unless otherwise specified. The resulting T-MA-T duplex displays a sigmoidal melting profile with elevated temperature, yielding a melting temperature (T_m) of approximately 45°C, as shown in Figure 2B. In the absence of MA cofactors, T21 existed as single random coils and did not exhibit a sigmoidal melting profile. However, when a 21-mer A-strand (A21) was introduced into the T-MA-T duplex, a new sigmoidal melting profile with an elevated T_m value of approximately 64°C was observed, corresponding to the formation of a base-paired A-T duplex. The nearly 20°C difference in T_m value between T-MA-T duplex and A-T duplex aligns with previous studies,[34] demonstrating the stronger binding affinity of Watson-Crick base pairing compared to MA-induced hydrogen bonding. These findings highlight the cascade of structural transitions undergone by T21: from a single random coil to the T-MA-T duplex upon the introduction of MA cofactors, and subsequently to the A-T duplex in the presence of A-strands.

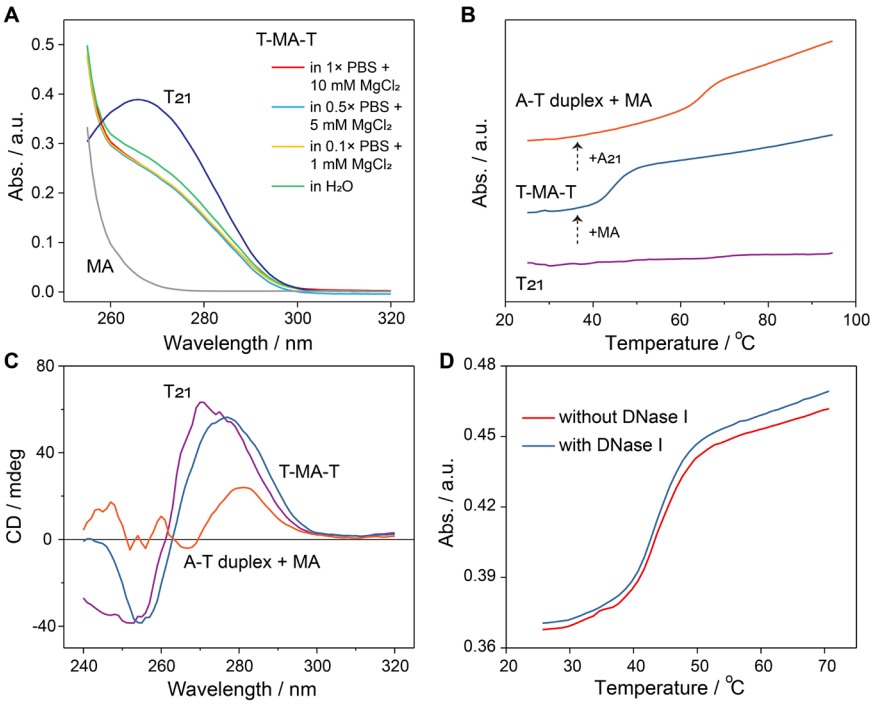

Figure 2. (A) Absorbance spectra of T21, MA and T-MA-T duplex under varying ionic strengths. (B) Melting profiles and (C) CD spectra of single T21 strands, T-MA-T duplex and A-T duplex. (D) Melting profiles of T-MA-T duplexes in the absence and presence of DNase I.

Additionally, the CD spectra of T21 were recorded with the sequential addition of MA cofactors and A-strands, as shown in Figure 2C. Upon the formation of the T-MA-T duplex, the positive peak of T21 exhibits a slight redshift along with a decrease in intensity. Following the introduction of A21, a further redshift of the positive peak is observed, indicating the replacement of MA cofactors in the T-MA-T duplex by A21 to form an A-T base-paired duplex. This positive peak closely resembles that of the A-T duplex in the absence of MA cofactors (Figure S1, Supporting Information), confirming the displacement of MA cofactors by A21. Notably, MA cofactors do not display any distinct CD peaks (Figure S1).

Moreover, the stability of T-MA-T duplex in the presence of cleavage enzyme, DNase I (preferentially cleaves double-stranded DNA by hydrolyzing phosphodiester bonds, producing oligonucleotides with 5'-phosphate ends), was studied. As shown in Figure 2D, the T-MA-T antiparallel duplex exhibits nearly identical melting profiles in both the absence and presence of DNase I (1 U), confirming its high resistance against nuclease cleavage.

The cascade configurational transitions were further analyzed using the fluorophore, thiazole orange (TO), whose fluorescence is significantly enhanced upon binding to rigid DNA duplexes.[38,39] As depicted in Figure 3A, TO features an asymmetric cyanine structure comprising conjugated benzothiazole and quinoline aromatic rings connected by a single methine bond. In its free state, intramolecular twisting motions lead to rapid non-radiative decay of the excited state, resulting in a non-fluorescent state (Figure S2). When free TO molecules were introduced to single T21 strands, minimal fluorescence is observed (Figure 3B). This behaviour can be attributed to the weak binding interaction between TO and the flexible single T21 strands in solution, which exerts minimal restriction on the free rotation of TO cofactors. Upon the MA cofactor-induced formation of the T-MA-T duplex, a significant enhancement in TO fluorescence at λ=540 nm is obtained (Figure 3C). This increase is due to the intercalation or stacking of TO molecules within the T-MA-T duplex, restricting their rotation along the methine bond and transitioning TO to a fluorescent state. Notably, neither MA cofactors alone nor the mixture of TO molecules and MA cofactors exhibits fluorescence within the 500-700 nm wavelength range (Figure S3 and S4). Subsequently, the introduction of A21 strands facilitated base-pairing hybridization, forming more rigid and energetically stable A-T duplexes. This structural rigidity further inhibited the free rotation of TO molecules (Figure 3D), resulting in higher fluorescence intensity compared to the T-MA-T duplex. These fluorescence results align with the preceding spectroscopy data,

reinforcing the evidence for cascade structural transitions: from single T21 strands to T-MA-T duplexes and ultimately to A-T duplexes.

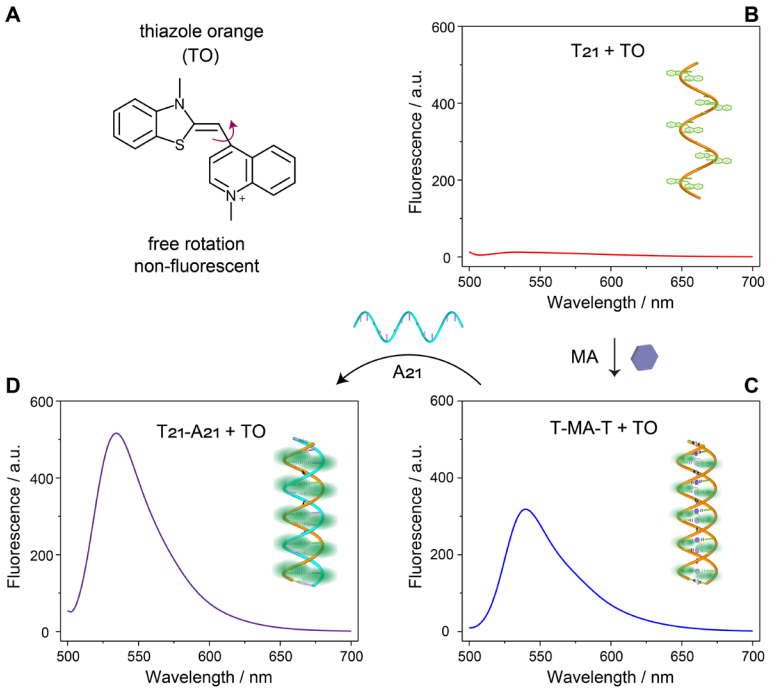

Figure 3. (A) Chemical structure of TO exhibiting free rotation along the methine bond. Fluorescence spectra of TO binding to single T21 strand (B), T-MA-T duplex (C) and A-T duplex (D).

To confirm whether the two T21 strands in the formed T-MA-T supramolecular structure adopt an antiparallel assembly, a fluorophore (Cyanine5, Cy5) and a quencher (Black Hole Quencher-2, BHQ-2) were conjugated to the 5'- and 3'-terminals of the T21 strand, respectively. In the absence of MA cofactors, the Cy5-T21-BHQ-2 strand shows medium fluorescence intensity at λ_{em}=664 nm when excited at λ_{ex}=645 nm, which can be attributed to the random coil configuration of the strand in solution (Figure 4A). However, upon the addition of MA cofactors into the system, the fluorescence intensity decreases significantly, resulting in minimal fluorescence. This quenching

effect is consistent with Förster resonance energy transfer (FRET), indicating spatial proximity between Cy5 and BHQ-2. Such a proximity strongly supports the antiparallel orientation of the two T21 strands in the T-MA-T supramolecular assembly. Notably, MA cofactors alone exhibit no fluorescence when excited at λ_{ex}=645 nm (Figure S5).

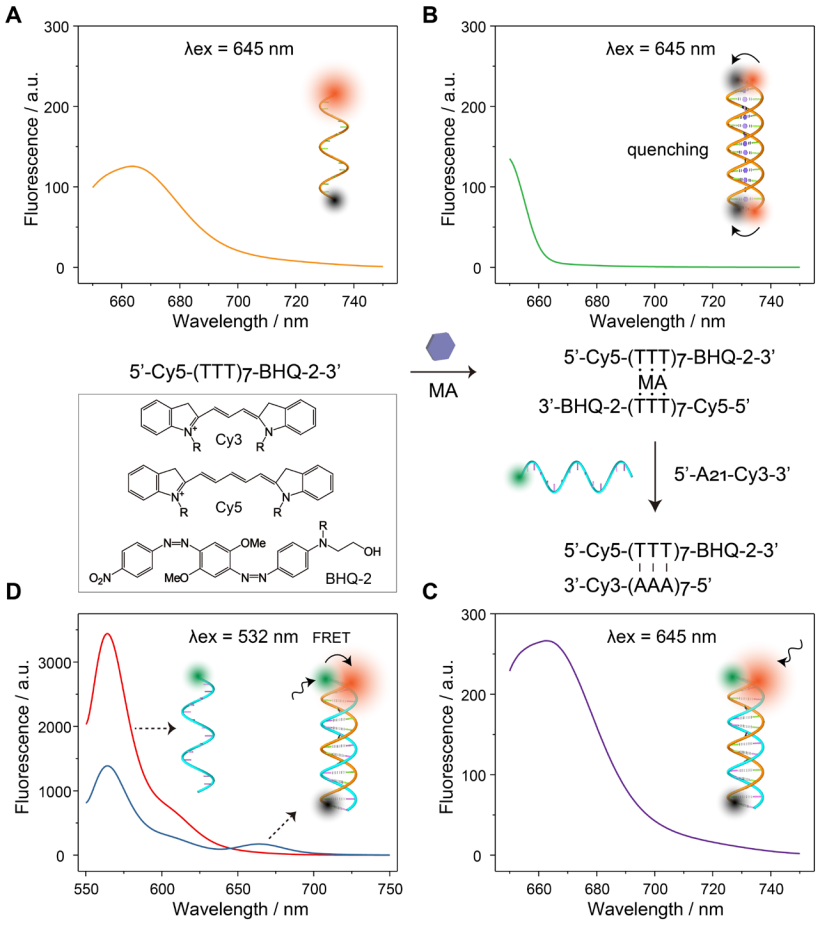

Figure 4. Fluorescence spectra of T21 strand with Cy5 and BHQ-2 modifications at 5'-terminal and 3'-terminal, respectively, (λ_{ex}=645 nm, A), MA mediated assembly into T-MA-T duplex (λ_{ex}=645 nm, B), and subsequent introduction of 3'-terminal Cy3 modified A21 strand, leading to the formation of T-A duplex with FRET (λ_{ex}=645 nm, C and λ_{ex}=532 nm, D).

Subsequently, the addition of A21 strands with Cyanine3 (Cy3) modification at its 3'-terminal into the T-MA-T duplex leads to an enhanced fluorescence of Cy5 when excited at λ_{ex}=645 nm (Figure 4C). The base-pairing interaction between T21 and A21 generated a rigid A-T duplex, separating the Cy5/BHQ-2 pair and restoring Cy5 fluorescence. The fluorescence intensity is higher than that observed in single T21 strands (Figure 4A), which exist as flexible random coils. This flexibility promotes FRET quenching between Cy5 and BHQ-2, unlike the rigid configuration of the A-T duplex. Additionally, excitation at λ_{ex}=532 nm revealed high fluorescence intensity of Cy3 modified A21 at λ_{em}=564 nm. However, in the formed A-T duplex, a significant reduction in fluorescence intensity at λ_{em}=564 nm and a corresponding increase at λ_{em}=664 nm are observed, demonstrating the FRET between Cy3 and Cy5 within the generated A-T duplex (Figure 4D). The UV-Vis spectra of the fluorophore- and quencher-modified sequences are presented in Figure S6. It should be noted that the A-T duplex formed both in the absence and presence of MA cofactors (Figure S7), highlighting the superior Watson-Crick base-pairing affinity compared to cofactor-induced hydrogen bonding. This distinction provides the foundation for subsequent DNA strand-triggered hydrogel phase transitions and payload release.

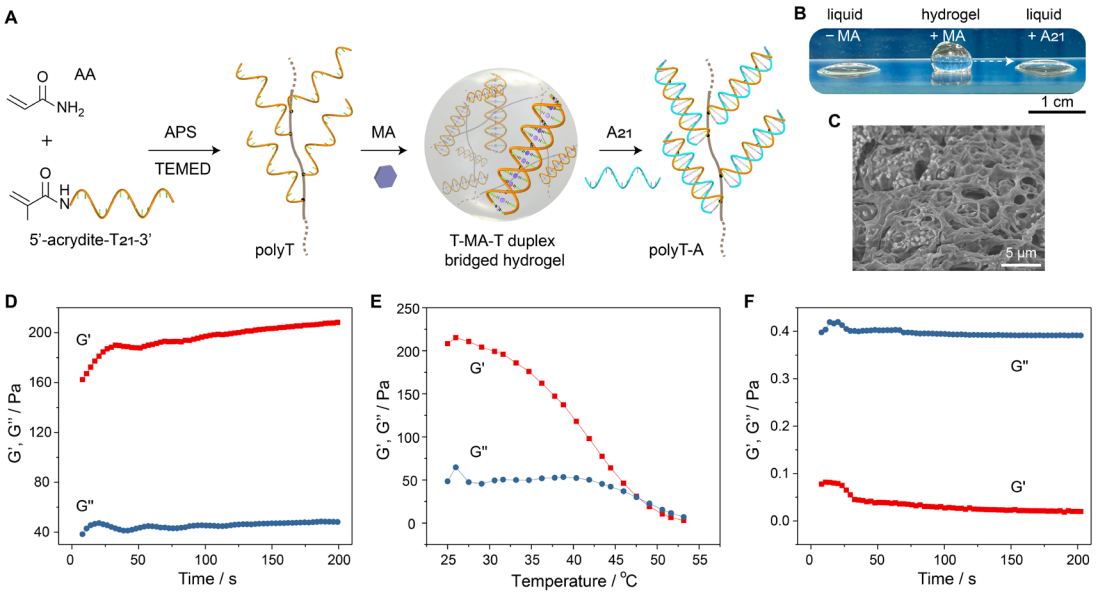

Figure 5. (A) Schematic presentation of synthesising the copolymer (polyT) with a polyacrylamide backbone and T21 tethers, the formation of the T-MA-T duplex-bridged DNA hydrogel upon addition of MA cofactors, and the subsequent dissociation of the DNA hydrogel upon introducing A21 strands, which hybridize with T21 to form polyT-A and displace the MA cofactors. (B) Photographs showing the transitions of polyT: liquid state (left), hydrogel state bridged by the T-MA-T duplex in the presence of MA cofactors (middle), and liquid state after the introduction of A21 (right). (C) SEM image of the T-MA-T duplex-bridged DNA hydrogel. (D, E) Rheological measurements of the T-MA-T duplex-bridged DNA hydrogel over time (D) and at elevated temperatures (E). (F) Rheological measurements of the liquid state after the introduction of A21 strands.

After confirming the sequential structural transitions from single T-strands to MA cofactor-mediated T-MA-T duplexes, followed by A-strand-induced A-T duplexes, these configurational properties were harnessed to develop a stimuli-responsive DNA hydrogel. As depicted in Figure 5A, 5'-terminal acrydite-modified T21 strands were copolymerized with acrylamide monomers in the presence of initiator ammonium persulphate (APS) and accelerator *N*,*N*,*N*′,*N*′-tetramethylethylenediamine (TEMED), yielding a copolymer termed polyT. The polyT copolymers, consisting of polyacrylamide backbones and T21 branches, existed in a liquid state due to the absence of crosslinking interactions. Upon introducing MA cofactors, the polyT copolymers formed a hydrogel state (Figure 5B), which was crosslinked by T-MA-T duplexes. Scanning electron microscopy (SEM) reveals the three-dimensional polymer networks with porous structures, as shown in Figure 5C. The white particles observed on the polymer surface are likely due to salts precipitation occurring during the hydrogel lyophilization process.

In the oscillation strain sweep test, the MA mediated polyT hydrogel exhibits a plateau region where the storage modulus (G') and loss modulus (G'') remain constant at low strain amplitudes, indicating the presence of a linear viscoelastic region (Figure S8).[40,41] In the oscillation frequency sweep test, the hydrogel shows higher G' values compared to G'' across the tested frequency range, confirming its gel-like characteristics (Figure S9).[40] The G'/G'' values also depend on the concentrations of T-strands in the copolymers. At a concentration of 0.5 mM, the G' value is 0.8 Pa and G'' value is 0.5 Pa (Figure S10), which was more a liquid state. At a concentration of 0.8 mM, it exhibited a hydrogel state with G' and G'' values of 50 Pa and 1.5 Pa, respectively (Figure S11). At a concentration of 1.2 mM, the G' and G'' values increased to approximately 200 Pa and 50 Pa, respectively (Figure 5D). When subjected to elevated temperatures, the T-MA-T bridged-hydrogel transitioned to a liquid state at approximately 50 °C (Figure 5E), demonstrating the disruption of the hydrogen bonding within the noncanonical duplex. It should be noted that batch-to-batch variations were observed (Figure S12), and an average value of 53±4.4 °C (n=3) was obtained. The polyT copolymers alone exhibited a liquid state with G' ≈ 0.03 Pa and G'' ≈ 0.06 Pa (Figure S13). Following the introduction of A21 strands into the T-MA-T duplex-crosslinked hydrogel, the system reverted to a liquid state (Figure 5B). The transition was attributed to the replacement of MA cofactors by A21 strands, forming A-T duplex (Figure 5A) and effectively breaking the hydrogel's bridging elements. The resulting liquid state exhibits a G' ≈ 0.05 Pa and G'' ≈ 0.4 Pa (Figure 5F).

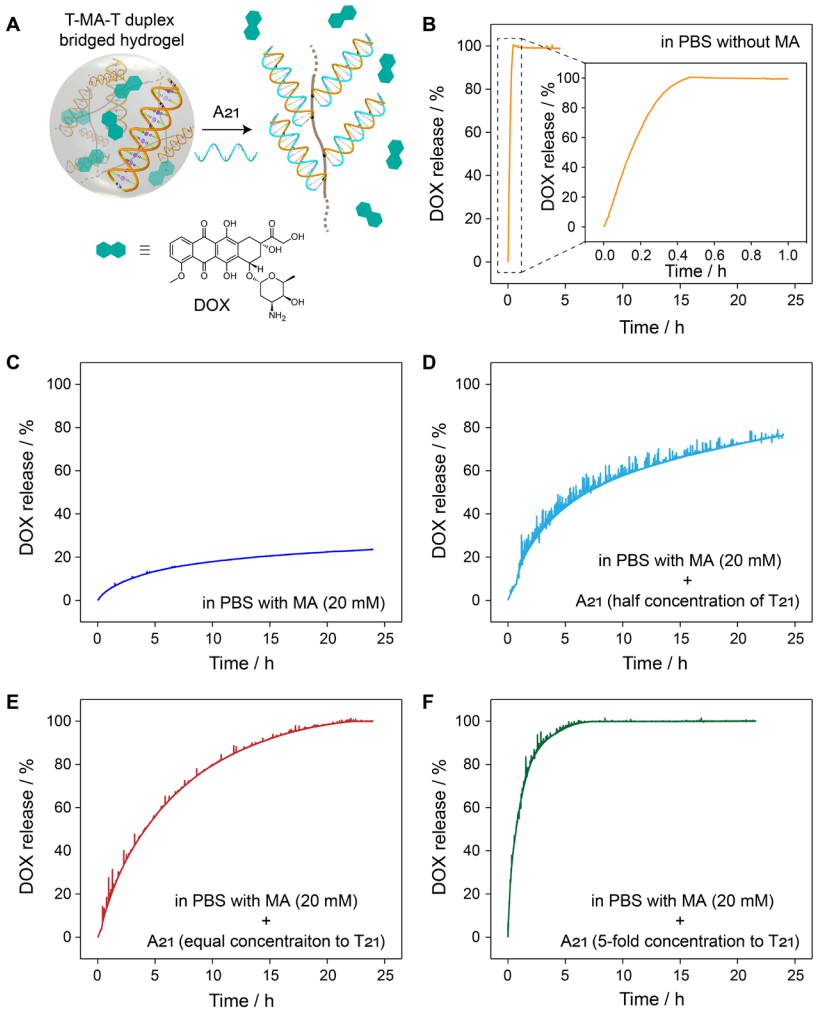

Figure 6. (A) Schematic demonstration of the A21-triggered disassembly of the T-MA-T duplex-bridged DNA hydrogel through the formation of A-T duplexes, accompanied by the release of DOX. Time-dependent release profiles of DOX from the T-MA-T duplex-bridged DNA hydrogel in: (B) PBS buffer without MA cofactors, (C) PBS buffer with MA cofactors, (D) PBS buffer with MA cofactors and A21 at half the concentration of T21 in the DNA hydrogel, (E) PBS buffer with MA cofactors and A21 at an equal concentration to T21 in the DNA hydrogel, (F) PBS buffer with MA cofactors and A21 at a 5-fold concentration relative to T21 in the DNA hydrogel.

The A21 strands induced phase transition from the T-MA-T duplex-crosslinked hydrogel state to a liquid state offers a mechanism for controlled payload release. To demonstrate this, the anticancer drug, doxorubicin (DOX), was encapsulated within the T-MA-T duplex-bridged hydrogel through intercalation or stacking interactions.[42] Upon the introduction of A21 strands, the formation of A-T duplex resulted in the disassembly of the hydrogel into a liquid state, facilitating the release of DOX (Figure 6A).

In DNA noncanonical structures generated by low-molecular-weight cofactors, such as the CA mediated A-CA triplex,[30] the concentration of cofactors is critical for the formation and stability of the induced configurations. This phenomenon was similarly observed in the current study. As depicted in Figure 6B, when the T-MA-T duplex-bridged hydrogel was placed in PBS buffer without MA cofactors, a rapid release of DOX was completed within 0.5 hours. The time-dependent release profiles of DOX from the hydrogel were monitored using UV-Vis spectroscopy at 496 nm, a characteristic absorption wavelength of DOX.[43] This behaviour is attributed to the concentration gradient between the MA cofactors within the hydrogel and the buffer solution, resulting in the diffusion of MA cofactors out of the T-MA-T duplexes into the buffer, leading to hydrogel dissociation due to insufficient cofactor concentration. Conversely, when the hydrogel was introduced into PBS buffer containing MA cofactors (Figure 6C), a minimal DOX release (or diffusion) of approximately 20% was observed over 24 hours, suggesting that the presence of MA cofactors in the buffer maintained the integrity of the T-MA-T duplex. Upon the introduction of A21 strands at a concentration equal to half that of T21 strands in the hydrogel, approximately 76% of the encapsulated DOX was released within 24 hours (Figure 6D). When the concentration of A21 strands was increased to match that of T21 strands in the hydrogel, complete release (100%) of DOX occurred within 24 hours (Figure 6E). This was due to the Watson-Crick base pairing

between A21 and T21 strands, which disrupted the T-MA-T duplex crosslinkers, resulting in full hydrogel dissociation. Further increasing the concentration of A21 strands to five times that of T21 strands accelerated the release rate, achieving complete DOX release within 7 hours (Figure 6F). These results demonstrate that by modulating the concentration of the trigger, A21 strands, the release rate of payloads (DOX) from the T-MA-T duplex-bridged hydrogel can be precisely controlled.

The payloads release from the T-MA-T duplex-bridged hydrogel involves the simultaneous release of MA cofactor. To assess the biocompatibility of the sample, cell cytotoxicity tests were conducted using primary human dermal fibroblasts. As shown in Figure S14 (Supporting Information), cell viability remained consistently high across MA concentrations ranging from 0 to 5 mM, with no significant reduction observed, indicating the sample's minimal toxicity.

CONCLUSION

In summary, we present cascade DNA structural transitions that progress from single strands to low-molecular-weight cofactor-induced noncanonical duplexes, and ultimately to canonical Watson-Crick duplex. Specifically, thymine-rich strands (T-strands) exist as random, flexible single coils in solution. Upon the introduction of melamine (MA) cofactors, which possess three adenine-like edges, a noncanonical antiparallel duplex, termed T-MA-T, is formed via hydrogen bonding between MA and thymine. Subsequently, when adenine-rich strands (A-strands) are introduced into the system, MA cofactors are replaced by A-strands in the T-MA-T configurations, resulting in the generation of the more energetically favourable Watson-Crick base-pairing canonical A-T duplex. These configurational transitions are further developed as bridging elements in a stimuli-responsive DNA hydrogel. An example drug, doxorubicin, is encapsulated

into the T-MA-T duplex-bridged hydrogel through intercalation or stacking interactions. Controlled hydrogel dissociation and drug release are achieved by introducing A-strands at varying concentrations or by the diffusion of MA cofactors from the noncanonical duplex in an MA-deficient environment. A-strands, which are tail components synthesized by polyA polymerase at the 3'-terminal of eukaryotic mRNA, play a critical role in mRNA stability and translation initiation. The further development of A-strands as triggers for the dissociation of T-MA-T duplex-bridged hydrogels could pave the way for the creation of intracellular mRNA-responsive platforms for controlled therapeutic delivery and gene regulation. For example, leveraging on the high stability of the T-MA-T duplex—its ability to form at low ionic strength and resist nuclease degradation—and scaling down the current system into nano/microplatforms such as nanogels or microcapsules, a promising strategy for mRNA-triggered bio-responsive platforms could be realized. This innovative framework for DNA structural transitions demonstrates its potential for stimuli-responsive material design and biomedical applications.

In the design of stimuli-responsive DNA hydrogels, various noncanonical DNA structures, such as G-quadruplexes, i-motifs, T-AT or C-GC triplexes, and A-motifs, have been employed due to their responsiveness to ions or pH changes.[44,45] Additionally, strategies based on DNA hybridization reactions[23] or aptamer-ligand interactions[46-48] have been integrated into hydrogel systems. For example, in aptamer-based mechanisms, aptamer strands are partially hybridized with blocker strands to form crosslinked polymer networks, resulting in a hydrogel state. Upon the introduction of a target ligand, specific aptamer-ligand binding disrupts the aptamer-bridged networks, leading to hydrogel dissociation and the release of encapsulated payloads. However, the hybridization domains of the aptamer must be carefully designed to ensure they do not interfere with subsequent ligand binding, adding complexity to the system. Furthermore, hybridized duplex

domains are susceptible to nuclease cleavage, which may lead to unintended payload release. In contrast, cofactor-mediated DNA structures, such as T-MA-T duplexes, offer a simpler and more robust alternative. Their formation is straightforward, and they exhibit resistance to nuclease degradation. Additionally, structural transitions in response to complementary A-strands occur in a direct and predictable manner. Moreover, the T-MA-T duplex utilizes two edges of the MA cofactor, leaving the third edge available for the introduction of additional functional groups, potentially enhancing versatility, biocompatibility and expanding functional applications.

EXPERIMENTAL SECTION

Materials. Magnesium chloride, ammonium persulfate, *N,N,N′,N′*-tetramethylethylenediamine, acrylamide solution (40%), melamine, thiazole orange, doxorubicin and other chemicals were purchased from Sigma-Aldrich, unless otherwise specified. All nucleic acid strands were purchased from Integrated DNA Technologies Inc. (Coralville, IA). Ultrapure water purified by a Milli-Q system was used to prepare all the solutions. The DNA sequences used in the study were:

T21: 5'- TTT TTT TTT TTT TTT TTT TTT -3'

A21: 5'- AAA AAA AAA AAA AAA AAA AAA -3'

Acrydite modified T21: 5'-acrydite- TTT TTT TTT TTT TTT TTT TTT -3'

Cy5-T21-BHQ-2: 5'-Cy5- TTT TTT TTT TTT TTT TTT TTT -BHQ-2-3'

Cy3-A21: 5'- AAA AAA AAA AAA AAA AAA AAA -Cy3-3'

UV–Vis spectra and melting curves. The UV–Vis spectra of samples were collected with Cary 3500 Compact Peltier UV–Vis Spectrophotometer (Agilent) equipped with a thermal controller component. The melting curves of samples were recorded with the absorbance at a wavelength of 260 nm by a temperature increment of 5 °C/min.

Fluorescence measurement. The fluorescence of TO (10 μM) was measured with T21 (2 μM) in the presence of MA (10 mM) in 1×PBS buffer (pH 7.2, containing 137 mM NaCl, 2.7 mM KCl, 10 mM Na_2HPO_4, 1.8 mM KH_2PO_4) with 10 mM $MgCl_2$. A21 of 2 μM was used to form A-T duplexes. For the control experiments, the same concentrations as above were adopted. The excitation wavelength for TO was 482 nm, and the spectrum was recorded in the wavelength range of 500–700 nm. For the FRET measurements, the concentrations of DNA strands were 3 μM. The excitation wavelengths for Cy3 and Cy5 were 532 nm and 645 nm, respectively. The measurements were conducted by fluorescence spectrophotometer (Hitachi, Model F-7100, Japan).

CD spectra. The CD spectra of T21 (16 μM) in the absence and presence of MA cofactors (50 mM) were recorded in 1×PBS buffer (pH 7.2) containing 10 mM $MgCl_2$ by JASCO J-815CD Spectrometer. In the A-T duplexes, the concentrations of T21 and A21 strands were both 8 μM, and the concentration of MA cofactors was 50 mM.

Synthesis of polyT copolymer. The synthesis and purification of polyT copolymer were conducted according to our previous study.[36]

Formation of the T-MA-T duplex-bridged hydrogel, DOX encapsulation, and triggered release. To generate the T-MA-T duplex-bridged DNA hydrogels, polyT (1.2 mM) and MA cofactors (20 mM) were used, annealed at 65 °C, and subsequently cooled to room temperature to induce the formation of a homogeneous hydrogel in 1×PBS buffer (pH 7.2, containing 10 mM $MgCl_2$). To achieve DOX encapsulation, 1 μL DOX (43 mM) was loaded into 10 μL hydrogel. Then the sample was transferred in 1×PBS buffer (pH 7.2, containing 10 mM $MgCl_2$) in the absence or presence of MA cofactors (20 mM) under constant stirring (300 rpm). The time-

dependent release profiles of DOX from the T-MA-T duplex-bridged hydrogel were recorded at a wavelength of 496 nm. For the A21 strands-triggered release, the concentrations of A21 added into the system were adjusted relative to the concentration of T21 strands in the hydrogel.

SEM imaging. SEM images were obtained with a field emission scanning electron microscope (JEOL JSM-6700F, Japan). According to the procedures, the DNA hydrogels were prepared, freeze-dried, and then coated with an Au/Pd film before imaging.

Rheological measurements. The mechanical properties of the T-MA-T duplex-bridged DNA hydrogel were characterized by an HAAKE™ MARS™ Rheometer (Thermo Scientific). The samples were placed onto a parallel-plate geometry (35 mm in diameter) at a temperature of 25 °C. The linear viscoelastic region was found to be in the range of 0.1 % strain and 1 Hz frequency.

Nuclease cleavage. The stability of T-MA-T duplexes against nuclease cleavage was examined by using DNase I (1 U, 30 min, New England Biolabs (NEB)). The melting profiles of T-MA-T duplexes (~2 μM) in the absence and presence of DNase I were recorded by UV–Vis Spectrophotometer.

Cytotoxicity test. The cytotoxicity of the sample was assessed using the CellTiter-Glo® 2.0 Cell Viability Assay (Promega). Sample test solution was prepared by dissolving sample in the cell culture medium at concentrations ranging from 0 to 5 mM. Primary human dermal fibroblasts (HDF, ATCC) were grown in DMEM enriched with 10% fetal bovine serum (Thermo Fisher Scientific) and 1% penicillin/streptomycin (Thermo Fisher Scientific), and incubated at 37 °C with 5% CO_2. The cells were subcultured with 0.05% trypsin-ethylenediaminetetraacetic acid once they reached 80% to 90% confluence. The cells were seeded in a 96-well plate with each well containing approximately 10^4 cells, and cultured for 24 h. Afterward, the media in the wells were

replaced with 100 μL of the prepared sample test solution, and the cells were then incubated for an additional 24 hours. A volume of 100 μL of assay reagent was added to each well for cell lysis. The plates were incubated at room temperature for 10 minutes to allow the luminescent signal to stabilize. Luminescence was then measured using a microplate reader (Cytation 1), and cell viability was calculated as a percentage relative to the control cells.

ASSOCIATED CONTENT

Supporting Information. Additional UV−Vis, CD, fluorescence spectra and rheology measurements, cell viability

AUTHOR INFORMATION

Corresponding Author

Yuwei Hu – Institute of Materials Research and Engineering (IMRE), Agency for Science, Technology and Research (A*STAR), 2 Fusionopolis Way, Innovis #08-03, 138634 Singapore, Republic of Singapore

*E-mail: ywhu@imre.a-star.edu.sg

Author Contributions

The manuscript was written through contributions of all authors. All authors have given approval to the final version of the manuscript. ‡These authors contributed equally.

Funding Sources

The research is supported by Career Development Fund (C210112014), SERC Central Research Fund (CRF, UIBR, KIMR220901aSERCRF), and RIE2025 Manufacturing, Trade, and

Connectivity (MTC) Programmatic Fund under grant M24M9b0013 entitled BLISS: Beyond Liquids with In-Situ Solid-state Surficial Sensorics, IMRE, A*STAR, Singapore.

Notes

The authors declare no competing financial interest.

ACKNOWLEDGMENT

The kind assistance with the SEM by Karen Tang Yuanting (IMRE) and the cell viability by Dr. Hongfang Lu (IMCB, A*STAR) is greatly appreciated.

REFERENCES

(1) Peters, R. J.; Marguet, M.; Marais, S.; Fraaije, M. W.; van Hest, J. C.; Lecommandoux, S. Cascade reactions in multicompartmentalized polymersomes. *Angew. Chem. Int. Ed.* **2014**, *53*, 146-150.

(2) Walsh, C. T.; Moore, B. S. Enzymatic Cascade Reactions in Biosynthesis. *Angew. Chem. Int. Ed.* **2019**, *58*, 6846-6879.

(3) Nicolaou, K. C.; Edmonds, D. J.; Bulger, P. G. Cascade reactions in total synthesis. *Angew. Chem. Int. Ed.* **2006**, *45*, 7134-7186.

(4) Wu, C.; Cansiz, S.; Zhang, L.; Teng, I. T.; Qiu, L.; Li, J.; Liu, Y.; Zhou, C.; Hu, R.; Zhang, T.; Cui, C.; Cui, L.; Tan, W. A Nonenzymatic Hairpin DNA Cascade Reaction Provides High Signal Gain of mRNA Imaging inside Live Cells. *J. Am. Chem. Soc.* **2015**, *137*, 4900-4903.

(5) Ren, K.; Xu, Y.; Liu, Y.; Yang, M.; Ju, H. A Responsive "Nano String Light" for Highly Efficient mRNA Imaging in Living Cells via Accelerated DNA Cascade Reaction. *ACS Nano* **2018**, *12*, 263-271.

(6) Han, D.; Wu, C.; You, M.; Zhang, T.; Wan, S.; Chen, T.; Qiu, L.; Zheng, Z.; Liang, H.; Tan, W. A cascade reaction network mimicking the basic functional steps of adaptive immune response. *Nat. Chem.* **2015**, *7*, 835-841.

(7) Hu, Y.; Wang, F.; Lu, C. H.; Girsh, J.; Golub, E.; Willner, I. Switchable enzyme/DNAzyme cascades by the reconfiguration of DNA nanostructures. *Chem. Eur. J.* **2014**, *20*, 16203-16209.

(8) Fu, J.; Yang, Y. R.; Johnson-Buck, A.; Liu, M.; Liu, Y.; Walter, N. G.; Woodbury, N. W.; Yan, H. Multi-enzyme complexes on DNA scaffolds capable of substrate channelling with an artificial swinging arm. *Nat. Nanotech.* **2014**, *9*, 531-536.

(9) Lin, P.; Dinh, H.; Morita, Y.; Nakata, E.; Morii, T. Dynamic Assembly of Cascade Enzymes by the Shape Transformation of a DNA Scaffold. *Adv. Funct. Mater.* **2023**, *33*, 2215023.

(10) Kou, B. B.; Chai, Y. Q.; Yuan, Y. L.; Yuan, R. A DNA nanopillar as a scaffold to regulate the ratio and distance of mimic enzymes for an efficient cascade catalytic platform. *Chem. Sci.* **2020**, *12*, 407-411.

(11) Fan, S.; Ji, B.; Liu, Y.; Zou, K.; Tian, Z.; Dai, B.; Cui, D.; Zhang, P.; Ke, Y.; Song, J. Spatiotemporal Control of Molecular Cascade Reactions by a Reconfigurable DNA Origami Domino Array. *Angew. Chem. Int. Ed.* **2022**, *61*, e202116324.

(12) Liu, F.; Li, N.; Shang, Y.; Wang, Y.; Liu, Q.; Ma, Z.; Jiang, Q.; Ding, B. A DNA-Based Plasmonic Nanodevice for Cascade Signal Amplification. *Angew. Chem. Int. Ed.* **2022**, *61*, e202114706.

(13) Maffeis, V.; Belluati, A.; Craciun, I.; Wu, D.; Novak, S.; Schoenenberger, C. A.; Palivan, C. G. Clustering of catalytic nanocompartments for enhancing an extracellular non-native cascade reaction. *Chem. Sci.* **2021**, *12*, 12274-12285.

(14) Wang, X.; Liu, L.; Wu, H.; Wu, Z.; Tang, L. J.; Jiang, J. H. Programming DNA cascade circuits on live cell membranes for accurate cancer cell recognition and gene silencing. *Chem. Commun.* **2021**, *57*, 3816-3819.

(15) Zhou, Z.; Ouyang, Y.; Wang, J.; Willner, I. Dissipative Gated and Cascaded DNA Networks. *J. Am. Chem. Soc.* **2021**, *143*, 5071-5079.

(16) Zhou, Z.; Lin, N.; Ouyang, Y.; Liu, S.; Zhang, Y.; Willner, I. Cascaded, Feedback-Driven, and Spatially Localized Emergence of Constitutional Dynamic Networks Driven by Enzyme-Free Catalytic DNA Circuits. *J. Am. Chem. Soc.* **2023**, *145*, 12617-12629.

(17) Yue, L.; Wang, S.; Zhou, Z.; Willner, I. Nucleic Acid Based Constitutional Dynamic Networks: From Basic Principles to Applications. *J. Am. Chem. Soc.* **2020**, *142*, 21577-21594.

(18) Lilienthal, S.; Luo, G. F.; Wang, S.; Yue, L.; Fischer, A.; Ehrlich, A.; Nahmias, Y.; Willner, I. Constitutional Dynamic Networks-Guided Synthesis of Programmed "Genes", Transcription of mRNAs, and Translation of Proteins. *J. Am. Chem. Soc.* **2020**, *142*, 21460-21468.

(19) Ouyang, Y.; Dong, J.; Willner, I. Dynamic DNA Networks-Guided Directional and Orthogonal Transient Biocatalytic Cascades. *J. Am. Chem. Soc.* **2023**, *145*, 22135-22149.

(20) Wang, C.; O'Hagan, M. P.; Neumann, E.; Nechushtai, R.; Willner, I. Integration of photocatalytic and dark-operating catalytic biomimetic transformations through DNA-based constitutional dynamic networks. *Nat. Commun.* **2021**, *12*, 4224.

(21) Del Grosso, E.; Franco, E.; Prins, L. J.; Ricci, F. Dissipative DNA nanotechnology. *Nat. Chem.* **2022**, *14*, 600-613.

(22) Wang, J.; Li, Z.; Willner, I. Dynamic Reconfigurable DNA Nanostructures, Networks and Materials. *Angew. Chem. Int. Ed.* **2023**, *62*, e202215332.

(23) Cangialosi, A.; Yoon, C.; Liu, J.; Huang, Q.; Guo, J.; Nguyen, T. D.; Gracias, D. H.; Schulman, R. DNA Sequence–Directed Shape Change of Photopatterned Hydrogels via High-Degree Swelling. *Science* **2017**, *357*, 1126-1130.

(24) Fern, J.; Schulman, R. Modular DNA strand-displacement controllers for directing material expansion. *Nat. Commun.* **2018**, *9*, 3766.

(25) Hu, Y.; Gao, S.; Lu, H.; Ying, J. Y. Acid-Resistant and Physiological pH-Responsive DNA Hydrogel Composed of A-Motif and i-Motif toward Oral Insulin Delivery. *J. Am. Chem. Soc.* **2022**, *144*, 5461-5470.

(26) Song, N.; Chu, Y.; Li, S.; Dong, Y.; Fan, X.; Tang, J.; Guo, Y.; Teng, G.; Yao, C.; Yang, D. Cascade dynamic assembly/disassembly of DNA nanoframework enabling the controlled delivery of CRISPR-Cas9 system. *Sci. Adv.* **2023**, *9*, eadi3602.

(27) Hu, Y.; Liu, J.; Ke, Y.; Wang, B.; Lim, J. Y. C.; Dong, Z.; Long, Y.; Willner, I. Oligo-Adenine and Cyanuric Acid Supramolecular DNA-Based Hydrogels Exhibiting Acid-Resistance and Physiological pH-Responsiveness. *ACS Appl. Mater. Interfaces* **2024**, *16*, 29235-29247.

(28) Hu, Y.; Ke, Y.; Willner, I. A pH-Cascaded DNA Hydrogel Mediated by Reconfigurable A-motif Duplex, i-Motif Quadruplex, and T·A-T Triplex Structures. *Adv. Funct. Mater.* **2023**, *33*, 2304966.

(29) Hu, Y.; Willner, I. Oligo-Adenine Derived Secondary Nucleic Acid Frameworks: From Structural Characteristics to Applications. *Angew. Chem. Int. Ed.* **2024**, *63*, e202412106.

(30) Avakyan, N.; Greschner, A. A.; Aldaye, F.; Serpell, C. J.; Toader, V.; Petitjean, A.; Sleiman, H. F. Reprogramming the Assembly of Unmodified DNA with a Small Molecule. *Nat. Chem.* **2016**, *8*, 368-376.

(31) Rizzuto, F. J.; Platnich, C. M.; Luo, X.; Shen, Y.; Dore, M. D.; Lachance-Brais, C.; Guarne, A.; Cosa, G.; Sleiman, H. F. A Dissipative Pathway for the Structural Evolution of DNA Fibres. *Nat. Chem.* **2021**, *13*, 843-849.

(32) Lachance-Brais, C.; Hennecker, C. D.; Alenaizan, A.; Luo, X.; Toader, V.; Taing, M.; Sherrill, C. D.; Mittermaier, A. K.; Sleiman, H. F. Tuning DNA Supramolecular Polymers by the Addition of Small, Functionalized Nucleobase Mimics. *J. Am. Chem. Soc.* **2021**, *143*, 19824-19833.

(33) Lachance-Brais, C.; Yao, C.; Reyes-Valenzuela, A.; Asohan, J.; Guettler, E.; Sleiman, H. F. Exceptional Nuclease Resistance of DNA and RNA with the Addition of Small-Molecule Nucleobase Mimics. *J. Am. Chem. Soc.* **2024**, *146*, 5811-5822.

(34) Li, Q.; Zhao, J.; Liu, L.; Jonchhe, S.; Rizzuto, F. J.; Mandal, S.; He, H.; Wei, S.; Sleiman, H. F.; Mao, H.; Mao, C. A poly(thymine)-melamine duplex for the assembly of DNA nanomaterials. *Nat. Mater.* **2020**, *19*, 1012-1018.

(35) Lachance-Brais, C.; Rammal, M.; Asohan, J.; Katolik, A.; Luo, X.; Saliba, D.; Jonderian, A.; Damha, M. J.; Harrington, M. J.; Sleiman, H. F. Small Molecule-Templated DNA Hydrogel with Record Stiffness Integrates and Releases DNA Nanostructures and Gene Silencing Nucleic Acids. *Adv. Sci.* **2023**, *10*, e2205713.

(36) Lee, S. R.; Ong, C. Y. J.; Wong, J. Y.; Ke, Y.; Dong, Z.; Lim, J. Y. C.; Hu, Y. Supramolecular oligo-thymine/melamine nanobridge-driven macroscopic engineering: reprogrammable hydrogels for multi-stimuli responsive architectures. *Chem. Eng. J.* **2024**, *497*, 154698.

(37) Hu, Y.; Cecconello, A.; Idili, A.; Ricci, F.; Willner, I. Triplex DNA Nanostructures: From Basic Properties to Applications. *Angew. Chem. Int. Ed.* **2017**, *56*, 15210-15233.

(38) Hovelmann, F.; Seitz, O. DNA Stains as Surrogate Nucleobases in Fluorogenic Hybridization Probes. *Acc. Chem. Res.* **2016**, *49*, 714-723.

(39) Nygren, J.; Svanvik, N.; Kubista, M. The Interactions Between the Fluorescent Dye Thiazole Orange and DNA. *Biopolymers* **1998**, *46*, 39-51.

(40) Du, X.; Bi, Y.; He, P.; Wang, C.; Guo, W. Hierarchically Structured DNA‐Based Hydrogels Exhibiting Enhanced Enzyme‐Responsive and Mechanical Properties. *Adv. Funct. Mater.* **2020**, *30*, 2006305.

(41) Du, X.; He, P. P.; Wang, C.; Wang, X.; Mu, Y.; Guo, W. Fast Transport and Transformation of Biomacromolecular Substances via Thermo-Stimulated Active "Inhalation-Exhalation" Cycles of Hierarchically Structured Smart pNIPAM-DNA Hydrogels. *Adv. Mater.* **2023**, *35*, e2206302.

(42) Du, K.; Xia, Q.; Heng, H.; Feng, F. Temozolomide-Doxorubicin Conjugate as a Double Intercalating Agent and Delivery by Apoferritin for Glioblastoma Chemotherapy. *ACS Appl. Mater. Interfaces* **2020**, *12*, 34599-34609.

(43) Liu, Y.; Zhang, X.; Zhou, M.; Nan, X.; Chen, X.; Zhang, X. Mitochondrial-Targeting Lonidamine-Doxorubicin Nanoparticles for Synergistic Chemotherapy to Conquer Drug Resistance. *ACS Appl. Mater. Interfaces* **2017**, *9*, 43498-43507.

(44) Kahn, J. S.; Hu, Y.; Willner, I. Stimuli-Responsive DNA-Based Hydrogels: From Basic Principles to Applications. *Acc. Chem. Res.* **2017**, *50*, 680-690.

(45) Hu, Y.; Ying, J. Y. Reconfigurable A-motif, i-Motif and Triplex Nucleic Acids for Smart pH-Responsive DNA Hydrogels. *Mater. Today* **2023**, *63*, 188-209.

(46) Zhao, L.; Li, L.; Yang, G.; Wei, B.; Ma, Y.; Qu, F. Aptamer functionalized DNA hydrogels: Design, applications and kinetics. *Biosens. Bioelectron.* **2021**, *194*, 113597.

(47) Yang, H.; Liu, H.; Kang, H.; Tan, W. Engineering target-responsive hydrogels based on aptamer-target interactions. *J. Am. Chem. Soc.* **2008**, *130*, 6320-6321.

(48) Li, F.; Tang, J.; Geng, J.; Luo, D.; Yang, D. Polymeric DNA hydrogel: Design, synthesis and applications. *Prog. Polym. Sci.* **2019**, *98*, 101163.

TOC graphic